A Robust Multi-Resolution Approach for Solving Fully Non-Linear Inverse Scattering Problems

M. Salucci, A. Polo, and A. Massa

Abstract

The solution of highly non-linear inverse scattering (*IS*) problems is dealt with in this work. More in detail, an innovative *IS* strategy is introduced to tackle the ill-posedness and non-linearity issues, allowing to remarkably overcome the limitations of state-fo-the-art methods based on the classical Lippmann-Schwinger Integral Equation (*LSIE*) formulation. It is based on the effective integration of a New Integral Equation (*NIE*) method with a multi-resolution scheme (i.e., the Iterative Multi-Scaling Approach - *IMSA*). The arising *IMSA-NIE* method is able to adaptively increase the resolution only in those sub-regions of the imaged domain where the presence of an unknown target has been previously detected. Moreover, it allows to robustly retrieve images of strong scatterers even in presence of significant noise components on the scattered field used to make the inversions. Numerical results are shown to validate the effectiveness of the approach under several operative conditions involving several signal-to-noise ratios and considering different values of relative permittivity of the unknown target.

Contents

1 List of Symbols

- $k = \frac{2\pi}{\lambda}$: Free-space wave-number;
- D: Investigation domain;
- L_D: Side of the investigation domain;
- $a = L_D \frac{\sqrt{2}}{2}$: Radius of the smallest circle containing D;
- $\mathbf{r} = (x, y)$: Position vector;
- $\tau(\mathbf{r})$: Contrast function;
- $\varepsilon_r(\mathbf{r})$: Relative permittivity;
- ε_0: Free-space permittivity;
- $\sigma(\mathbf{r})$: Conductivity;
- Ξ: Reconstruction error;
- V: Number of views/sources;
- φ^v: Direction of the v-th plane wave ($v = 1, ..., V$);
- M: Number of measurement points;
- ρ: Radius of the measurement domain;
- N: Number of discretization cells inside D;
- Γ: Number of degrees-of-freedom of the scattered field;
- U: Number of retrievable unknowns;
- η: $IMSA$ Stopping threshold;
- S: Maximum number of $IMSA$ iterations;
- $L^{(s)}$: Side of the region of interest (RoI) at the s-th $IMSA$ step ($s = 1, ..., S$);
- K: Number of singular values used by the SOM to retrieve the minimum-norm currents;
- α: Threshold for the adaptive selection of the number of singular values;
- χ_m: m-th Singular value of the scattering operator ($m = 1, ..., M$);
- MF: Number of Fourier bases;
- β: NIE regularization parameter;
- γ: Multiplicative factor for the adaptive computation of β;
- I: Number of iterations;

2 Numerical Assessment

2.1 "Double L" Profile - Variation of SNR and $\varepsilon_{r,obj}$

Investigation domain (D)

- Side: $L_D = 3.0$ [λ];

Measurement setup

- Views
  - Type: plane wave with unitary magnitude;
  - Frequency: $f = 300$ [MHz];
  - Wavelength: $\lambda = 1.0$ [m];
  - Number of $DOFs$: $\Gamma = 2ka = 2k\left(L_D\frac{\sqrt{2}}{2}\right) = 4\frac{\pi}{\lambda}\left(L_D\frac{\sqrt{2}}{2}\right) \simeq 26.64$;
  - Number of views: $V = 27$;
  - Direction: $\varphi_v = (v-1)\,\frac{360}{V}$; $v = 1, ..., V$;
- Measurement points
  - Radius: $\rho = a = \left(L_D\frac{\sqrt{2}}{2}\right) = 2.12$ [λ];
  - Number of probes: $M = 27$;
  - Location: $(x_m,\, y_m) = \left(\rho\cos\left((m-1)\,\frac{2\pi}{M}\right),\, \rho\sin\left((m-1)\,\frac{2\pi}{M}\right)\right)$; $m = 1, ..., M$;

Scatterer

- Type: Double L
- Dielectric characteristics:

$\varepsilon_{r,obj}$	σ_{obj} [S/m]	$\Re\{\tau\}$	$\Im\{\tau\}$
1.5	0.0	0.5	0.0
2.0	0.0	1.0	0.0
3.0	0.0	2.0	0.0
4.0	0.0	3.0	0.0

Table I: "Double L" - Considered contrasts.

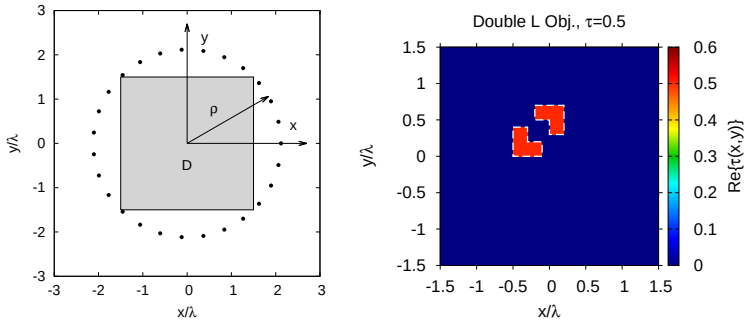

(*a*) (*b*)

Figure 1: "Double L Profile", $\tau = 0.5$ - (*a*) Imaging scenario and (*b*) actual dielectric profile.

Forward solver (MoM)

- Discretization: $N^{fwd} = 60 \times 60 = 3600$;
- Side of each cell: $l^{fwd} \simeq 0.05$ [λ];

Inverse solver

1. $IMSA - SOM - NIE$
   - Number of retrievable unknowns: $U = \frac{(2ka)^2}{2} = 4\pi^2 \left(\frac{L}{\lambda}\right)^2 = 355$;
   - Discretization: $N^{IMSA} = 18 \times 18 = 324$;
   - Side of each cell @ $s = 1$: $l_{s=1} = 0.17$ [λ];
   - Maximum number of steps: $S = 4$;
   - $IMSA$ stop criterion: adaptive ($\eta = 0.2$);
   - Selection of the singular values: adaptive;
   - Threshold for the adaptive selection of the number of singular values: $\alpha = 0.4$ (calibrated);
   - Number of Fourier bases: $MF = \frac{\sqrt{N^{IMSA}}}{2} = 9$ (standard SOM);
   - Selection of the NIE regularization parameter: adaptive;
   - Multiplicative factor for the selection of the NIE regularization parameter: $\gamma = 0.5$ (calibrated);
   - Number of iterations: $I = 100$.
2. $BARE - SOM - NIE$
   - Discretization: $N^{BARE} = 30 \times 30 = 900$;
   - Side of each cell: $l = 0.1$ [λ];
   - Number of singular values: $K = 15$ (non-adaptive);
   - Number of Fourier bases: $MF = \frac{\sqrt{N^{BARE}}}{2} = 15$ (standard SOM);
   - NIE regularization parameter: $\beta = 2.0$ (non-adaptive, calibrated);

- Number of iterations: $I = 100$.

3. $IMSA - SOM - CSI$

   - Same parameters of $IMSA - SOM - NIE$;
   - Threshold for the adaptive selection of the number of singular values: $\alpha = 0.7$ [1];

4. $BARE - SOM - CSI$

   - Same parameters of $BARE - SOM - NIE$;

Signal to noise ratio

- $SNR = \{10;\ 20;\ 40; 60\}$ [dB].

2.1.1 $\varepsilon_r = 1.5$, $\sigma = 0.0$ [S/m] $\rightarrow \tau = 0.5$

$IMSA - SOM - NIE$ **vs.** $BARE - SOM - NIE$**: Final reconstructions**

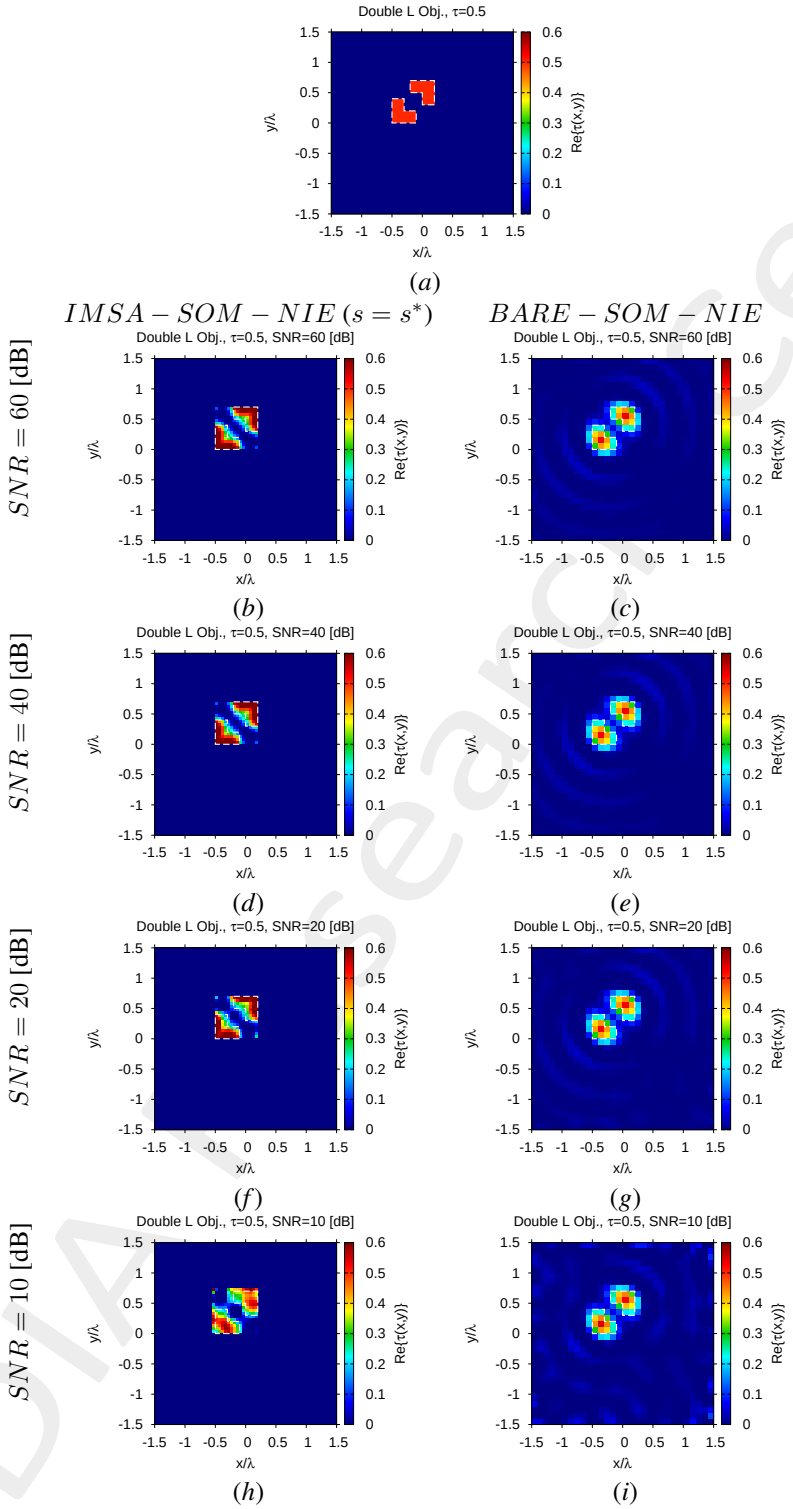

Figure 2: "Double L" Profile, $\tau = 0.5$ - (a) Actual and (b)-(i) retrieved contrast by the $IMSA - SOM - NIE$ and $BARE - SOM - NIE$ methods under several noise levels.

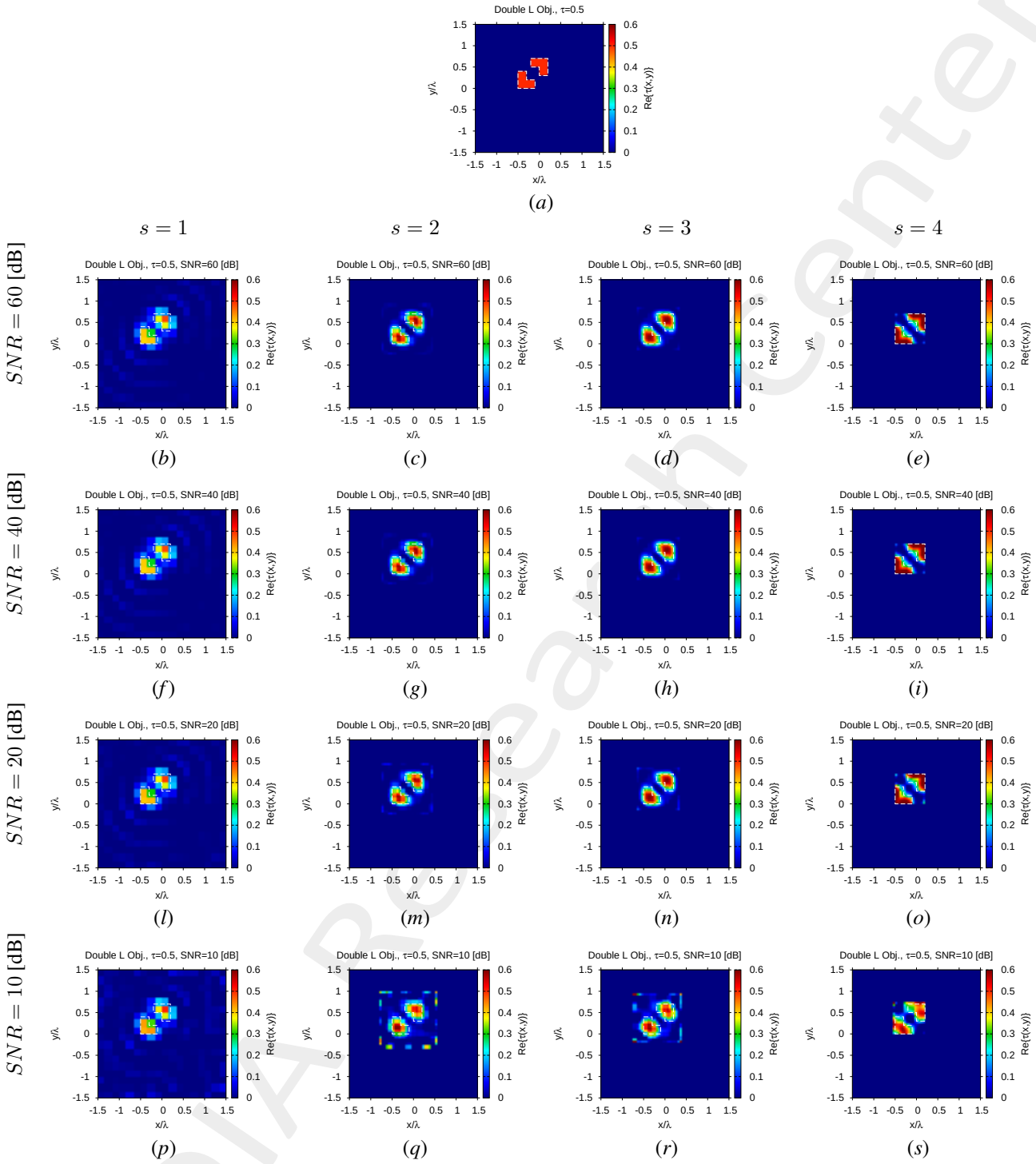

Figure 3: "Double L" Profile, $\tau = 0.5$ - (a) Actual and (b)-(i) intermediate retrieved contrast by the $IMSA-SOM-NIE$ under several noise levels.

$IMSA - SOM - CSI$ **vs.** $BARE - SOM - CSI$**: Final reconstructions**

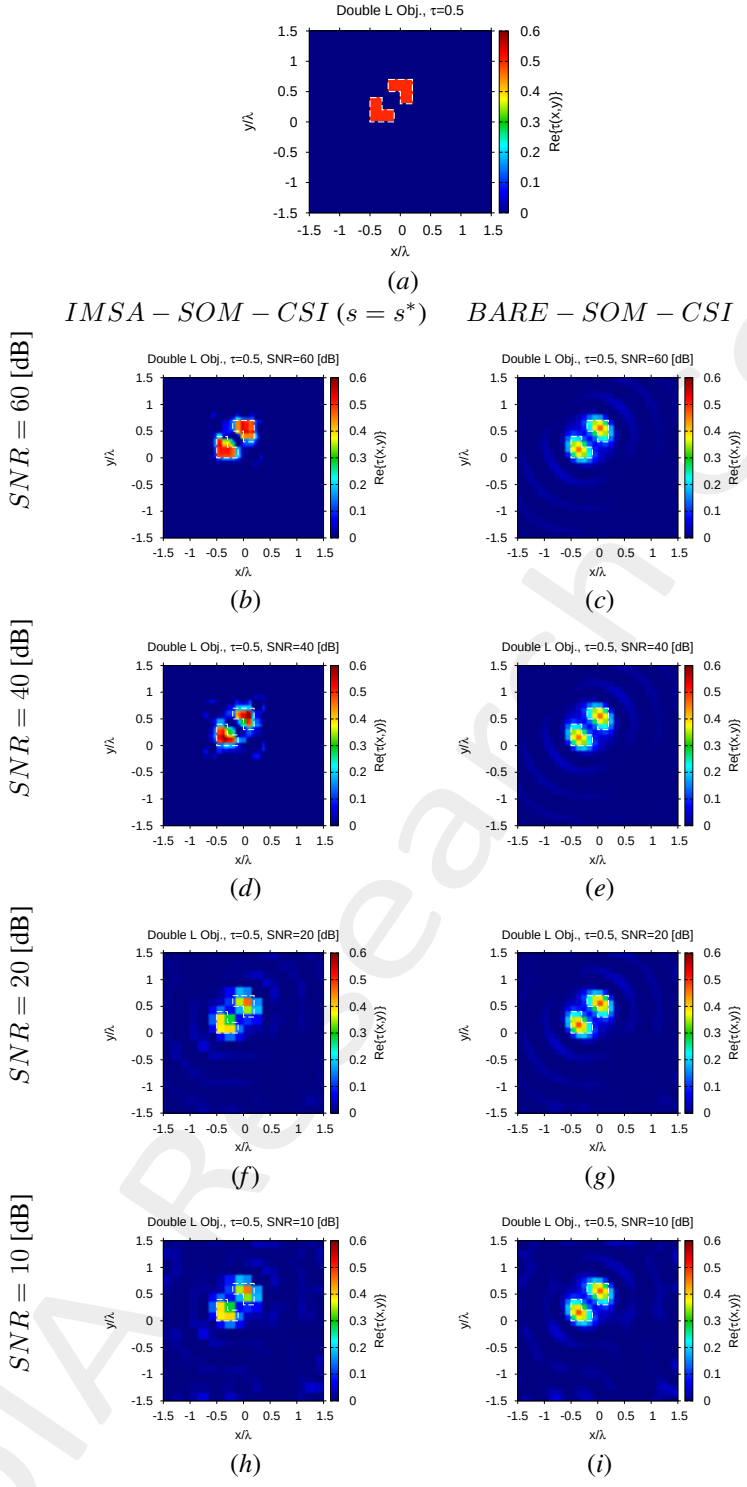

Figure 4: "Double L" Profile, $\tau = 0.5$ - (*a*) Actual and (*b*)-(*i*) retrieved contrast by the $IMSA - SOM - CSI$ and $BARE - SOM - CSI$ methods under several noise levels.

Reconstruction Errors vs. SNR

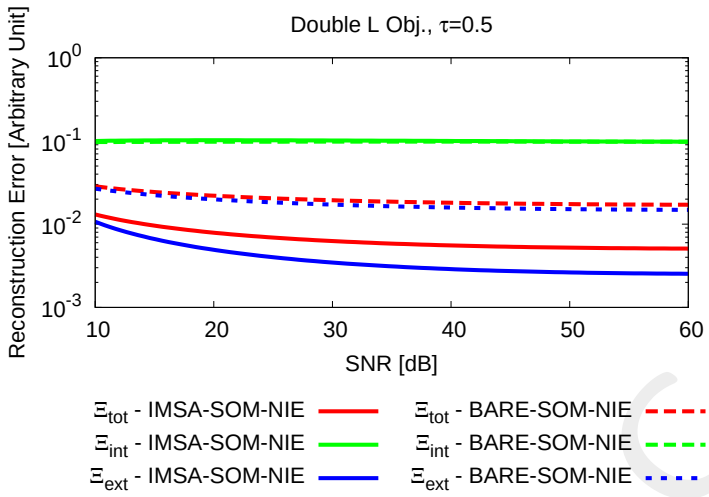

Figure 5: "Double L" Profile, $\tau = 0.5$ - Reconstruction errors for the $IMSA-SOM-NIE$ and $BARE-SOM-NIE$ methods.

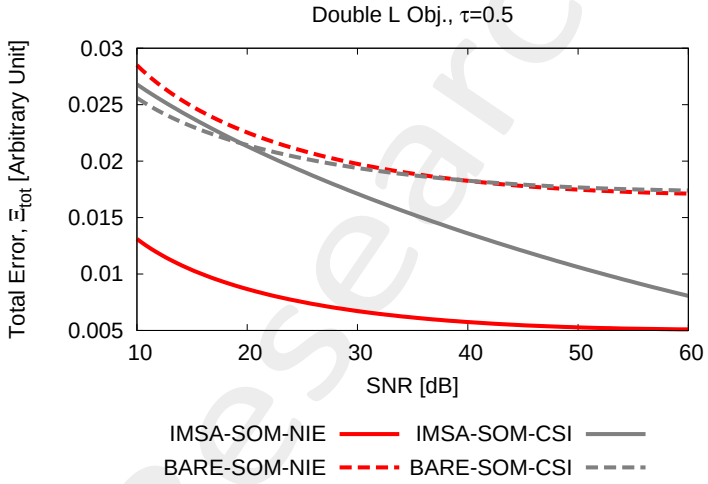

Figure 6: "Double L" Profile, $\tau = 0.5$ - Total error for $IMSA - SOM - NIE$, $BARE - SOM - NIE$, $IMSA - SOM - CSI$, and $BARE - SOM - CSI$.

2.1.2 $\varepsilon_r = 2.0, \sigma = 0.0$ **[S/m]** $\rightarrow \tau = 1.0$

$IMSA - SOM - NIE$ **vs.** $BARE - SOM - NIE$**: Final reconstructions**

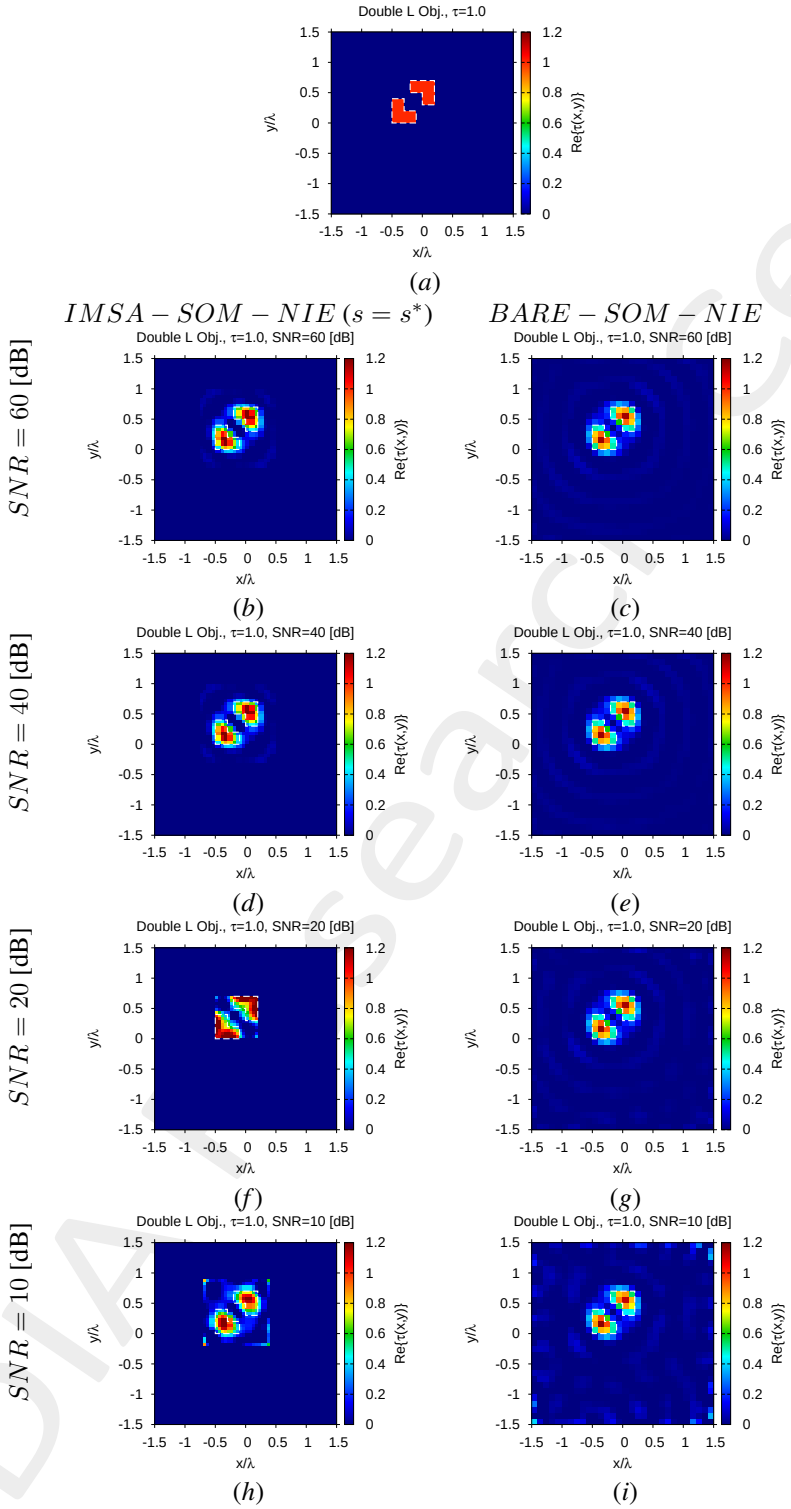

Figure 7: "Double L" Profile, $\tau = 1.0$ - (*a*) Actual and (*b*)-(*i*) retrieved contrast by the $IMSA - SOM - NIE$ and $BARE - SOM - NIE$ methods under several noise levels.

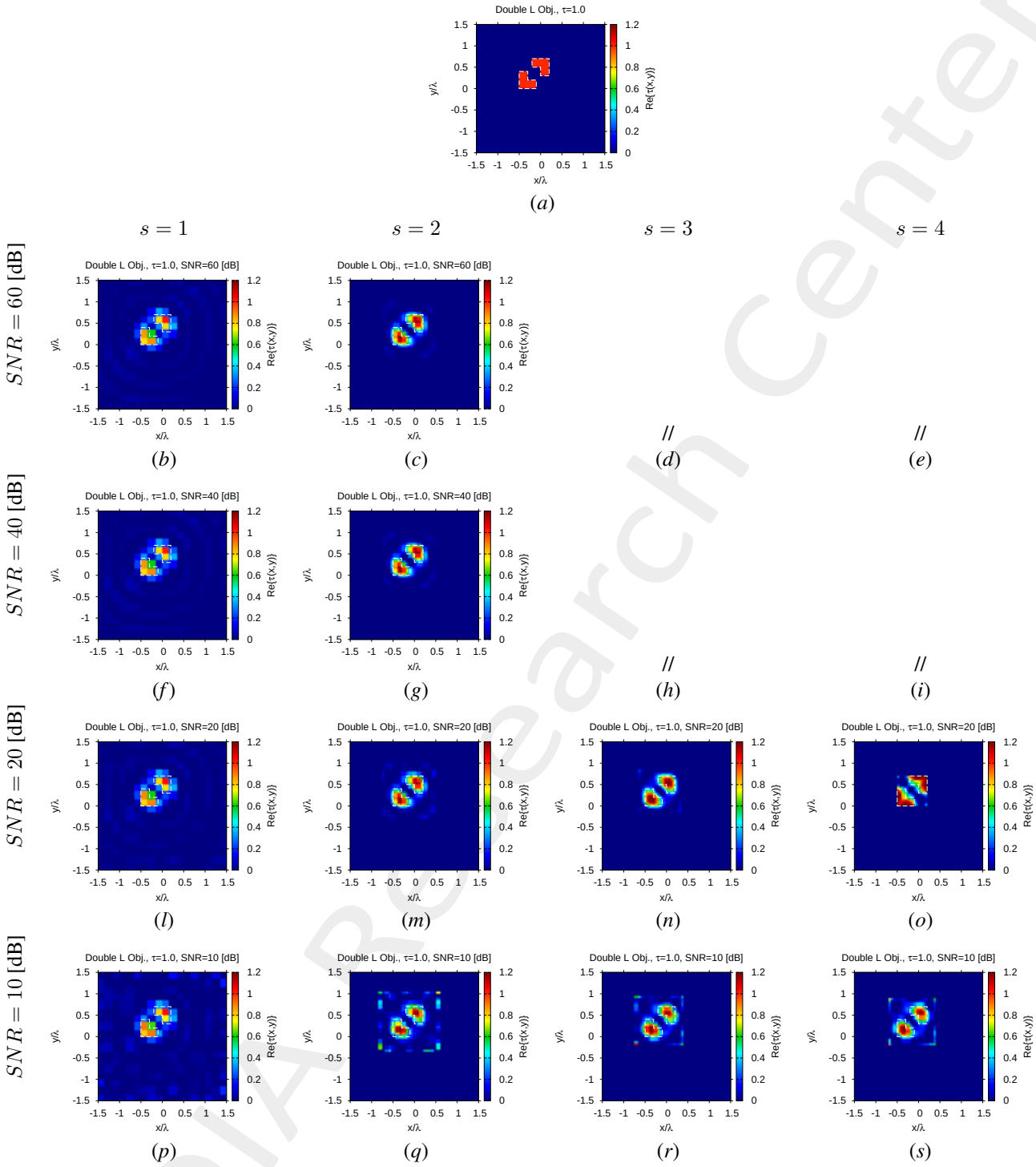

Figure 8: "Double L" Profile, $\tau = 1.0$ - (a) Actual and (b)-(i) intermediate retrieved contrast by the $IMSA-SOM-NIE$ under several noise levels.

$IMSA - SOM - CSI$ **vs.** $BARE - SOM - CSI$**: Final reconstructions**

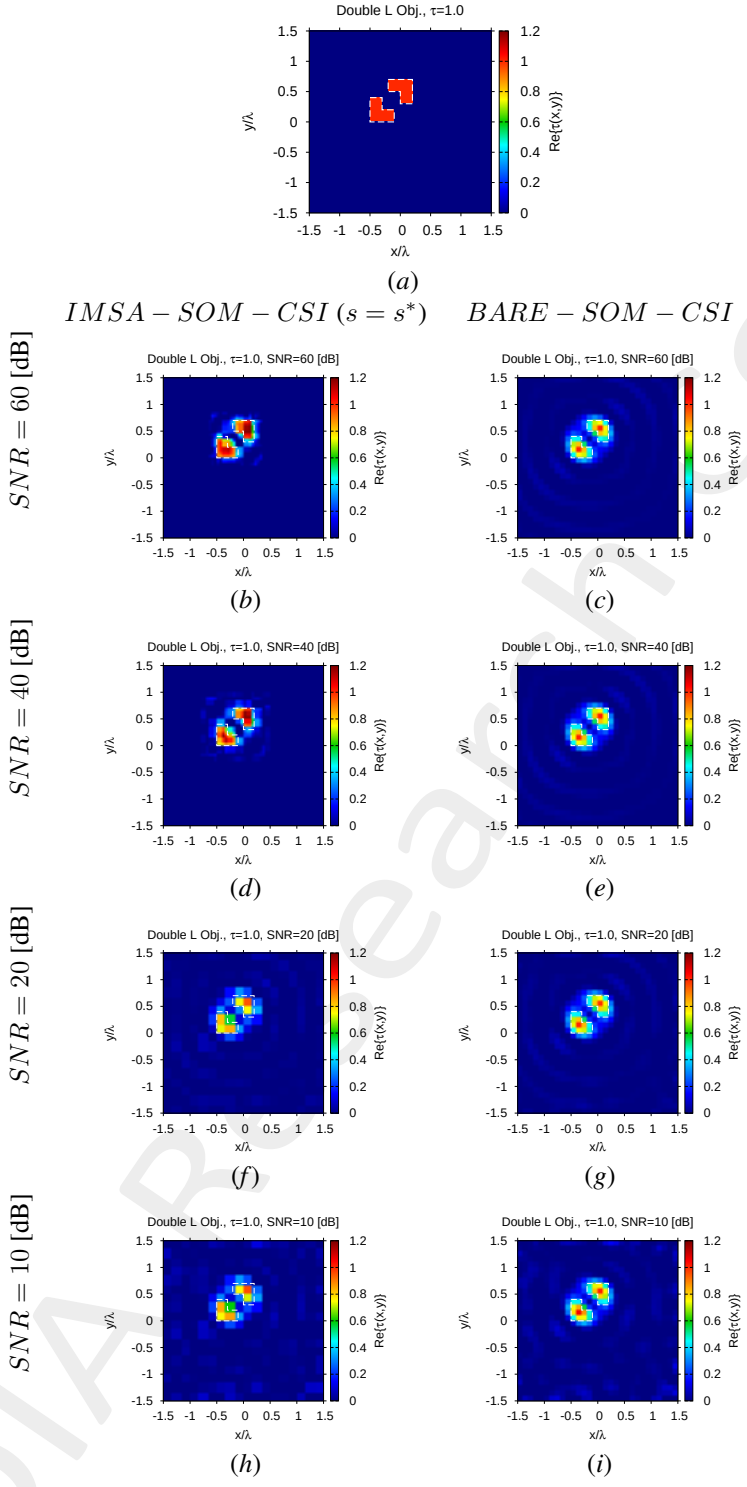

Figure 9: "Double L" Profile, $\tau = 1.0$ - (*a*) Actual and (*b*)-(*i*) retrieved contrast by the $IMSA - SOM - CSI$ and $BARE - SOM - CSI$ methods under several noise levels.

Reconstruction Errors vs. SNR

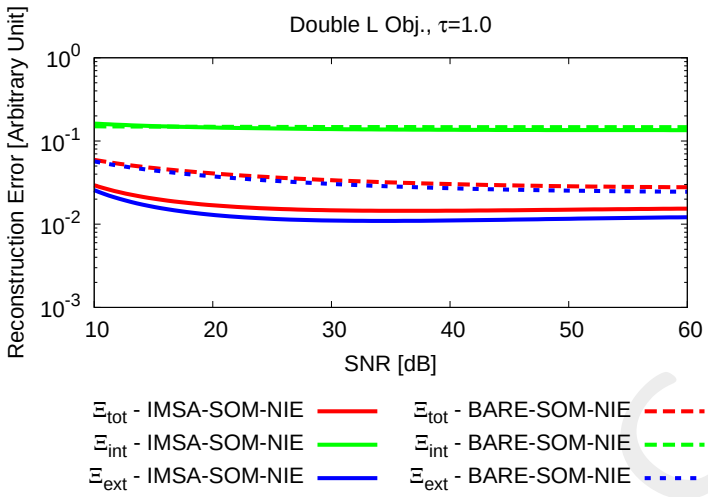

Figure 10: "Double L" Profile, $\tau = 1.0$ - Reconstruction errors for the $IMSA-SOM-NIE$ and $BARE-SOM-NIE$ methods.

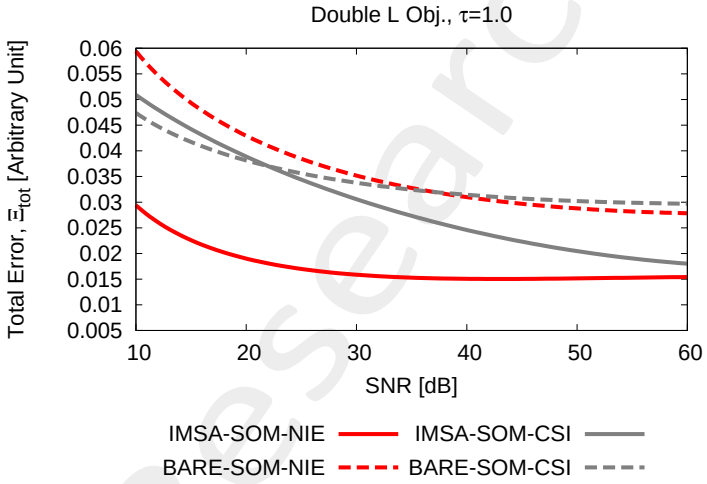

Figure 11: "Double L" Profile, $\tau = 1.0$ - Total error for $IMSA - SOM - NIE$, $BARE - SOM - NIE$, $IMSA - SOM - CSI$, and $BARE - SOM - CSI$.

2.1.3 $\varepsilon_r = 3.0, \sigma = 0.0$ **[S/m]** $\rightarrow \tau = 2.0$

$IMSA - SOM - NIE$ **vs.** $BARE - SOM - NIE$**: Final reconstructions**

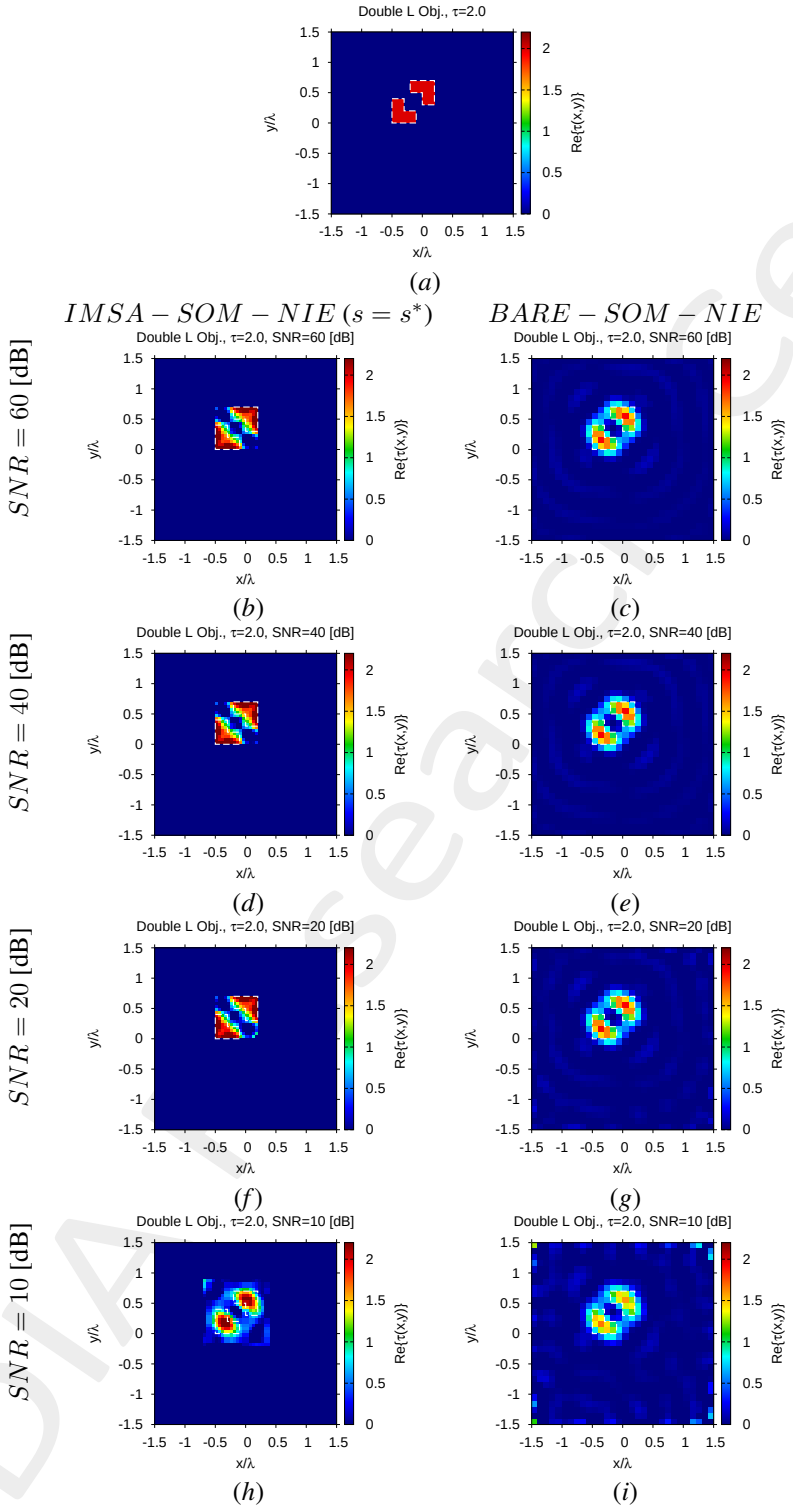

Figure 12: "Double L" Profile, $\tau = 2.0$ - (a) Actual and (b)-(i) retrieved contrast by the $IMSA - SOM - NIE$ and $BARE - SOM - NIE$ methods under several noise levels.

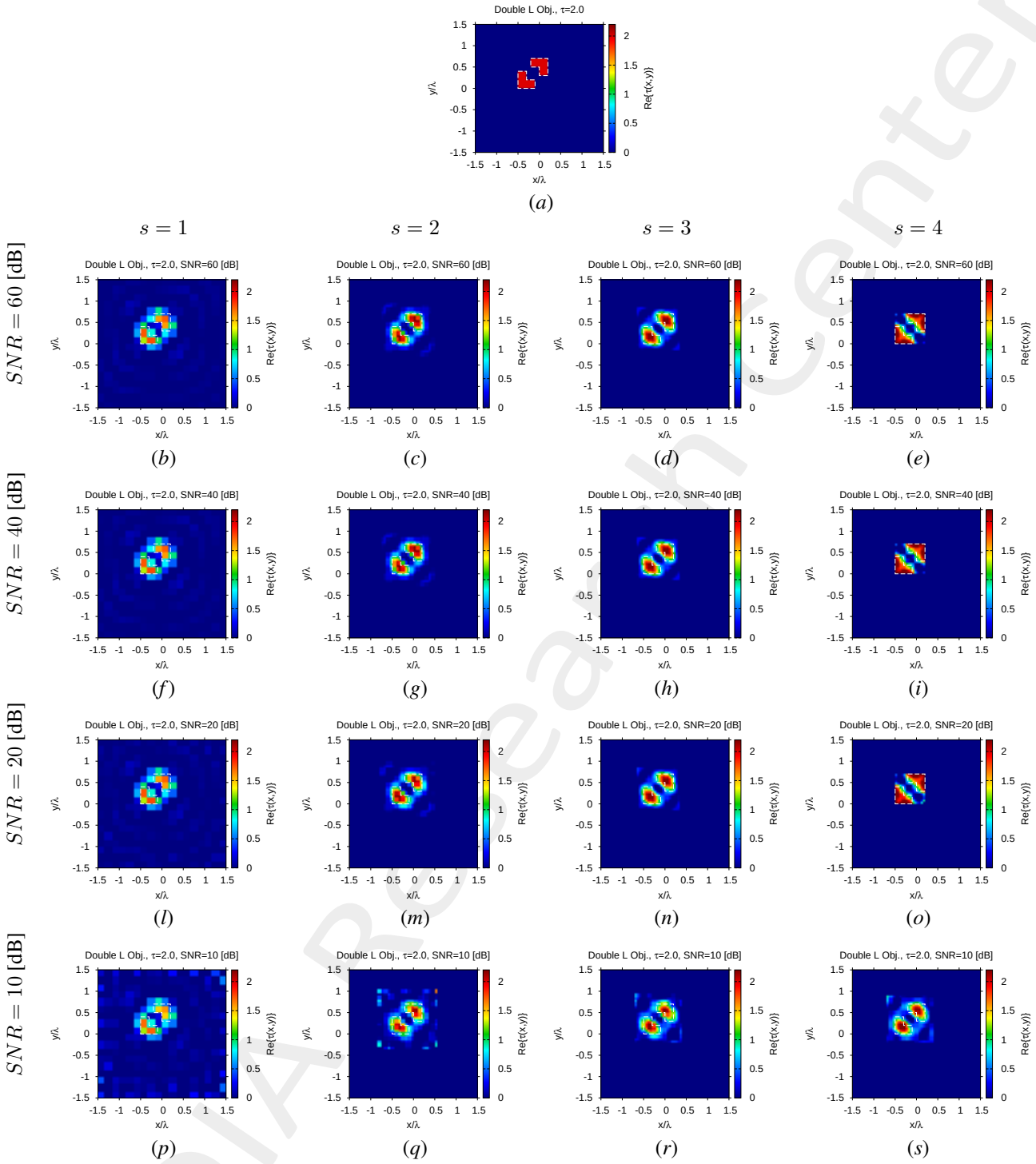

Figure 13: "Double L" Profile, $\tau = 2.0$ - (a) Actual and (b)-(i) intermediate retrieved contrast by the $IMSA - SOM - NIE$ under several noise levels.

$IMSA - SOM - CSI$ **vs.** $BARE - SOM - CSI$**: Final reconstructions**

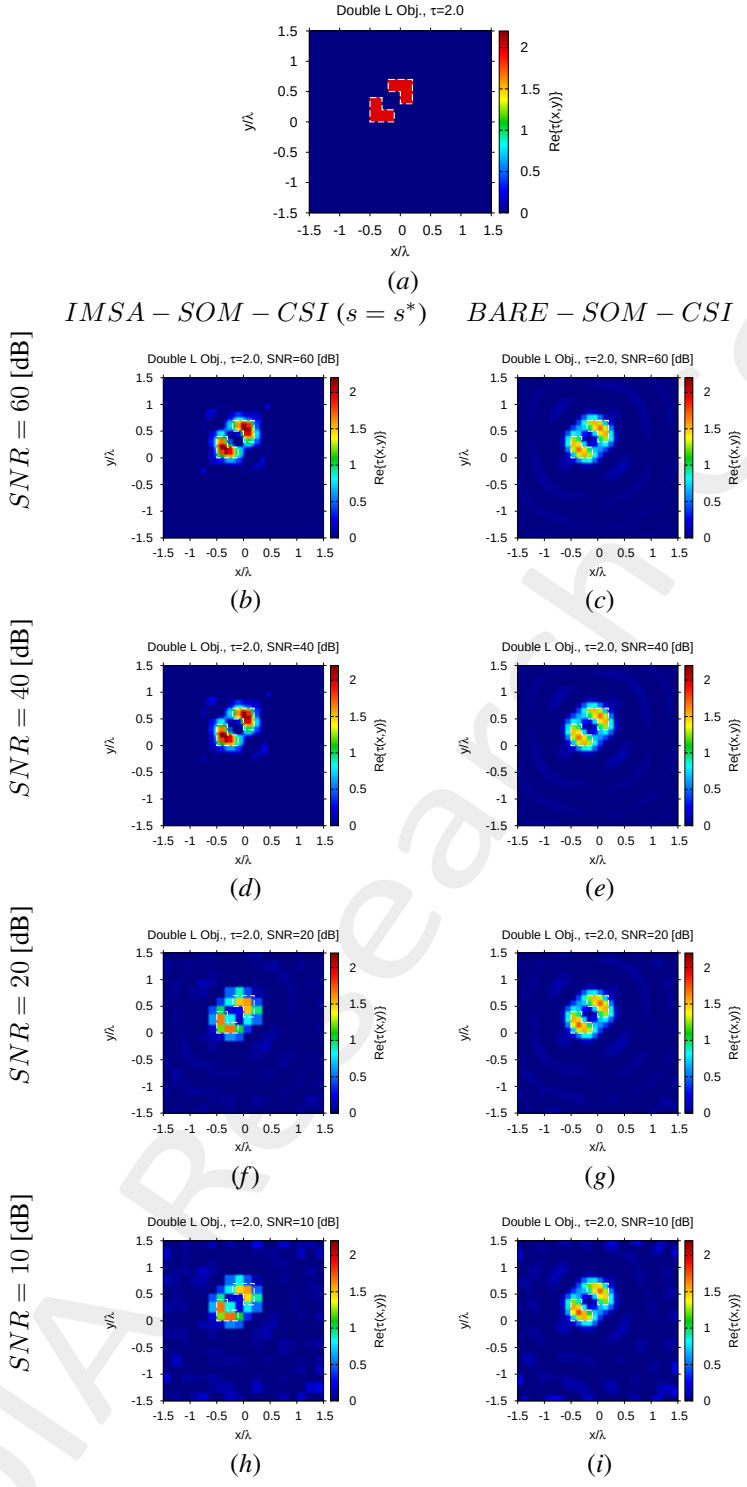

Figure 14: "Double L" Profile, $\tau = 2.0$ - (*a*) Actual and (*b*)-(*i*) retrieved contrast by the $IMSA - SOM - CSI$ and $BARE - SOM - CSI$ methods under several noise levels.

Reconstruction Errors vs. SNR

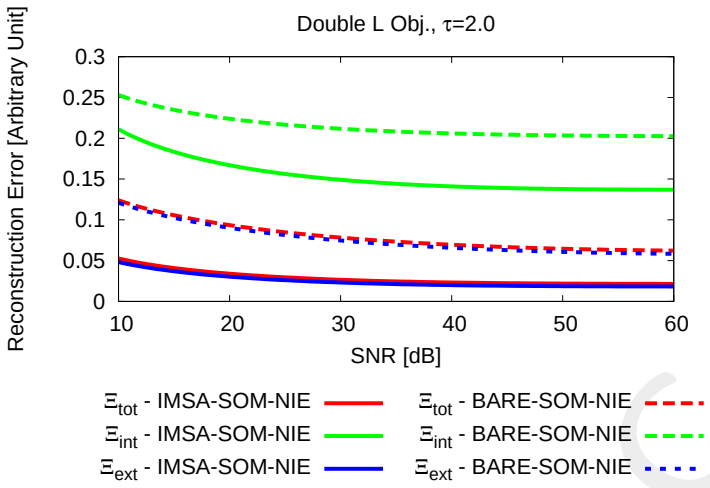

Figure 15: "Double L" Profile, $\tau = 2.0$ - Reconstruction errors for the $IMSA-SOM-NIE$ and $BARE-SOM-NIE$ methods.

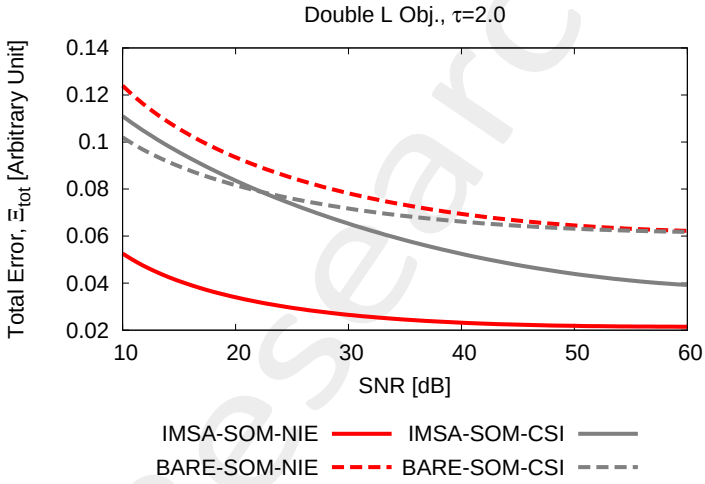

Figure 16: "Double L" Profile, $\tau = 2.0$ - Total error for $IMSA - SOM - NIE$, $BARE - SOM - NIE$, $IMSA - SOM - CSI$, and $BARE - SOM - CSI$.

2.1.4 $\varepsilon_r = 4.0$, $\sigma = 0.0$ **[S/m]** $\rightarrow \tau = 3.0$

$IMSA - SOM - NIE$ **vs.** $BARE - SOM - NIE$**: Final reconstructions**

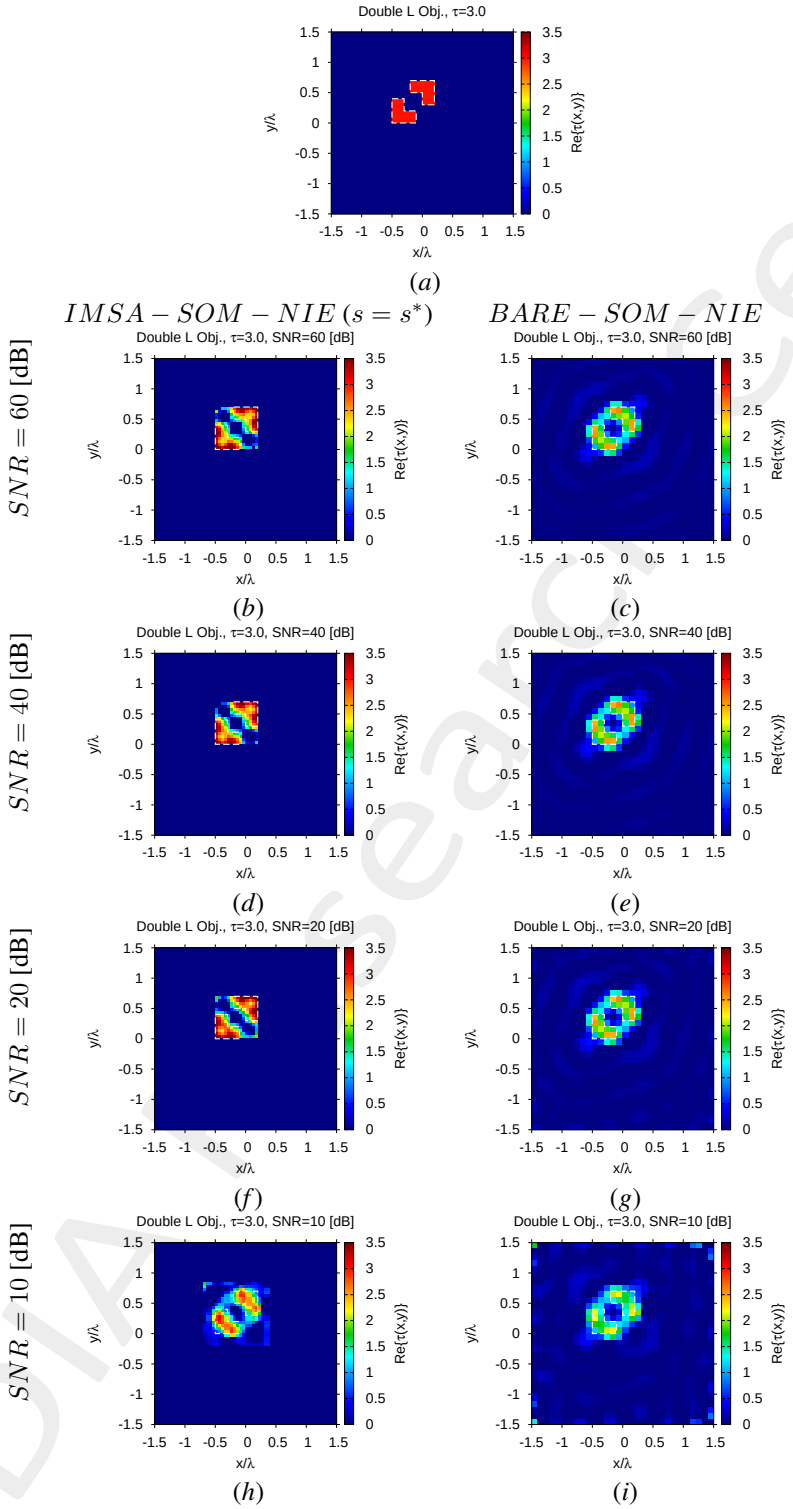

Figure 17: "Double L" Profile, $\tau = 3.0$ - (a) Actual and (b)-(i) retrieved contrast by the $IMSA - SOM - NIE$ and $BARE - SOM - NIE$ methods under several noise levels.

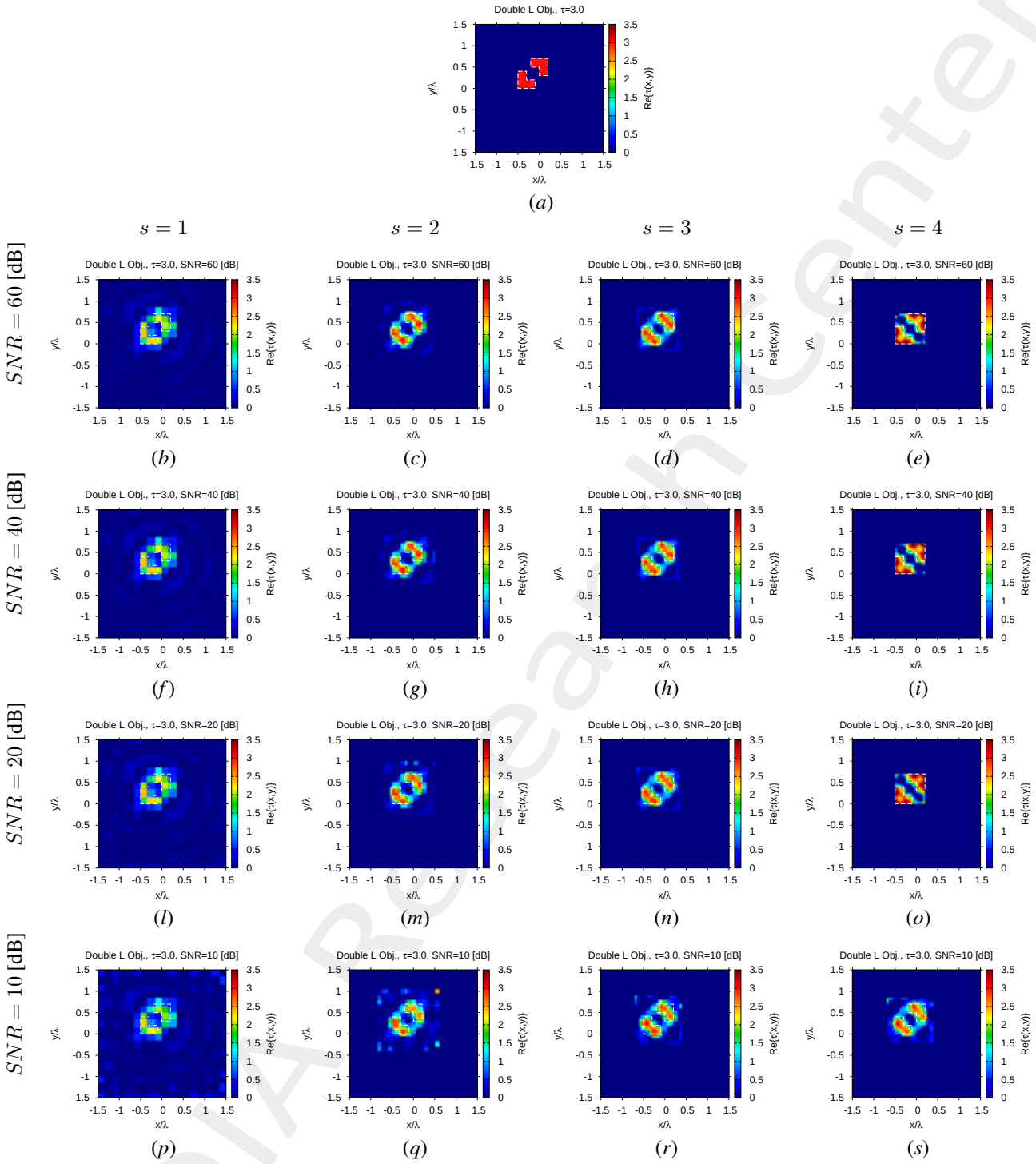

Figure 18: "Double L" Profile, $\tau = 3.0$ - (a) Actual and (b)-(i) intermediate retrieved contrast by the $IMSA - SOM - NIE$ under several noise levels.

$IMSA - SOM - CSI$ **vs.** $BARE - SOM - CSI$**: Final reconstructions**

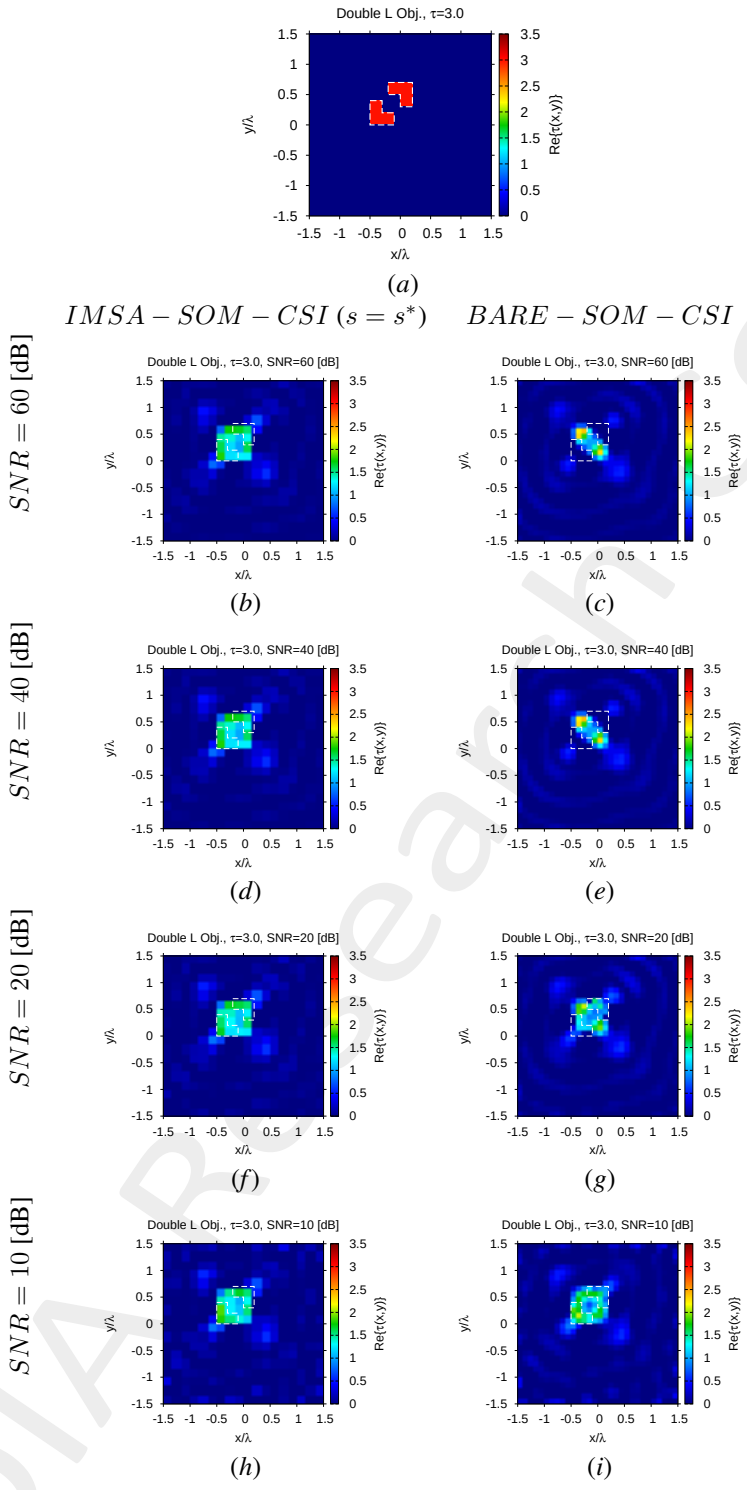

Figure 19: "Double L" Profile, $\tau = 3.0$ - (a) Actual and (b)-(i) retrieved contrast by the $IMSA - SOM - CSI$ and $BARE - SOM - CSI$ methods under several noise levels.

Reconstruction Errors vs. SNR

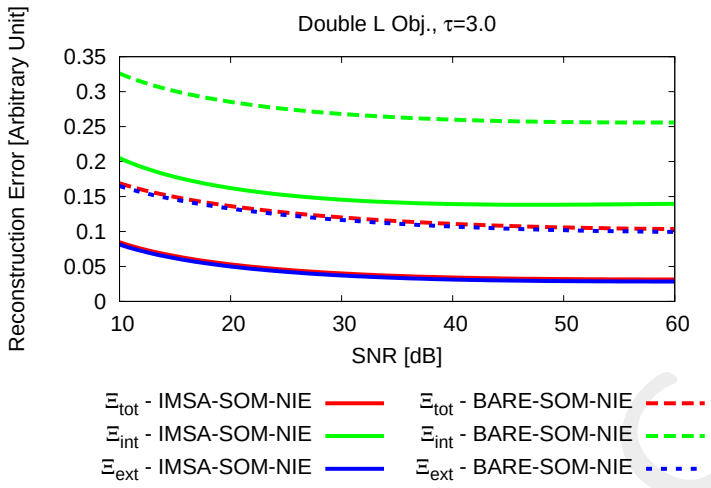

Figure 20: "Double L" Profile, $\tau = 3.0$ - Reconstruction errors for the $IMSA-SOM-NIE$ and $BARE-SOM-NIE$ methods.

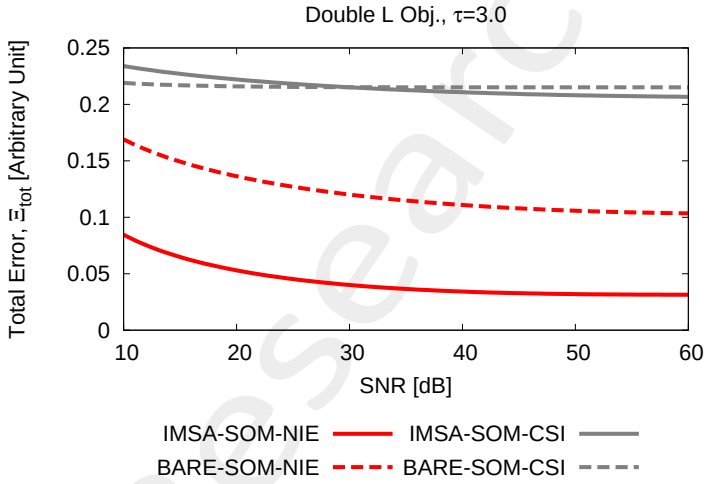

Figure 21: "Double L" Profile, $\tau = 3.0$ - Total error for $IMSA - SOM - NIE$, $BARE - SOM - NIE$, $IMSA - SOM - CSI$, and $BARE - SOM - CSI$.

2.2 Reconstruction Errors vs. $\Re\{\tau\}$

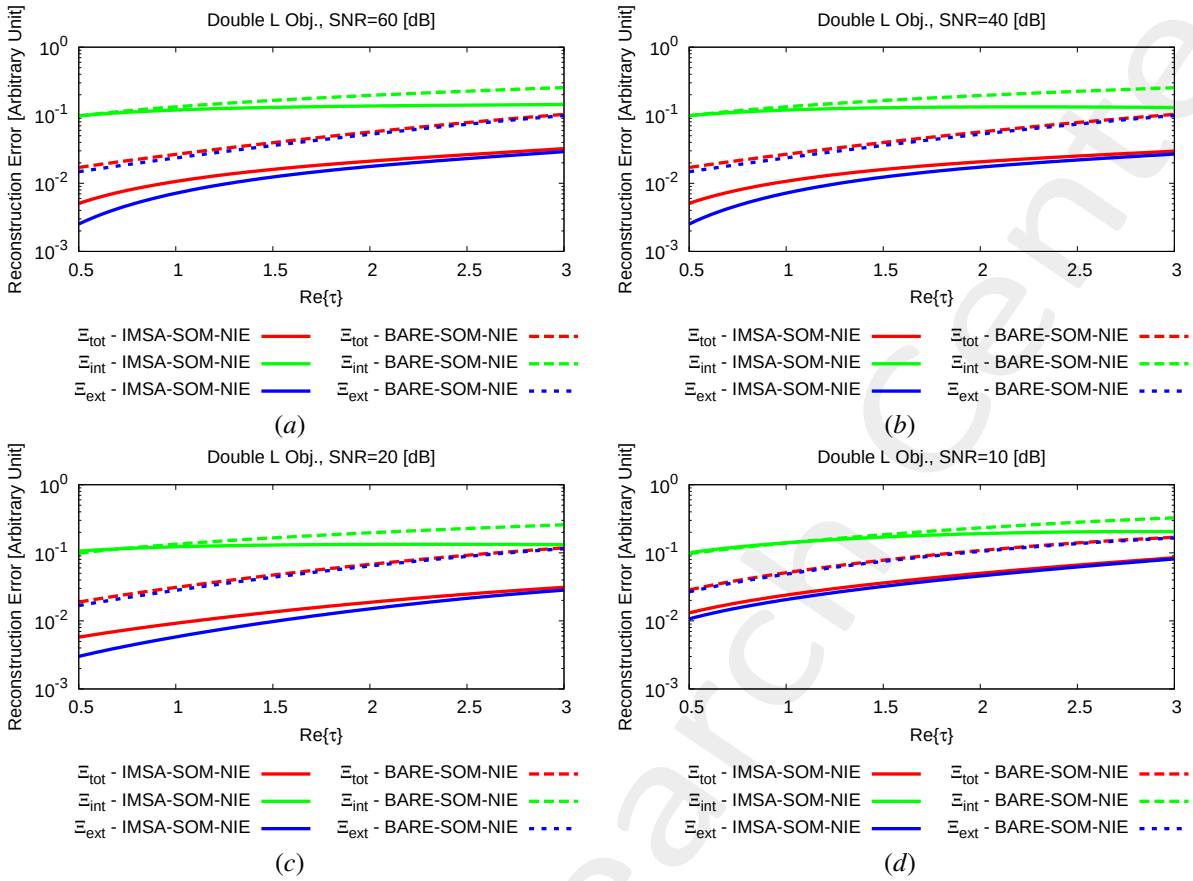

Figure 22: "Double L" Profile - Reconstruction errors vs. $\Re\{\tau\}$ for the $IMSA-SOM-NIE$ and $BARE-SOM-NIE$ methods.

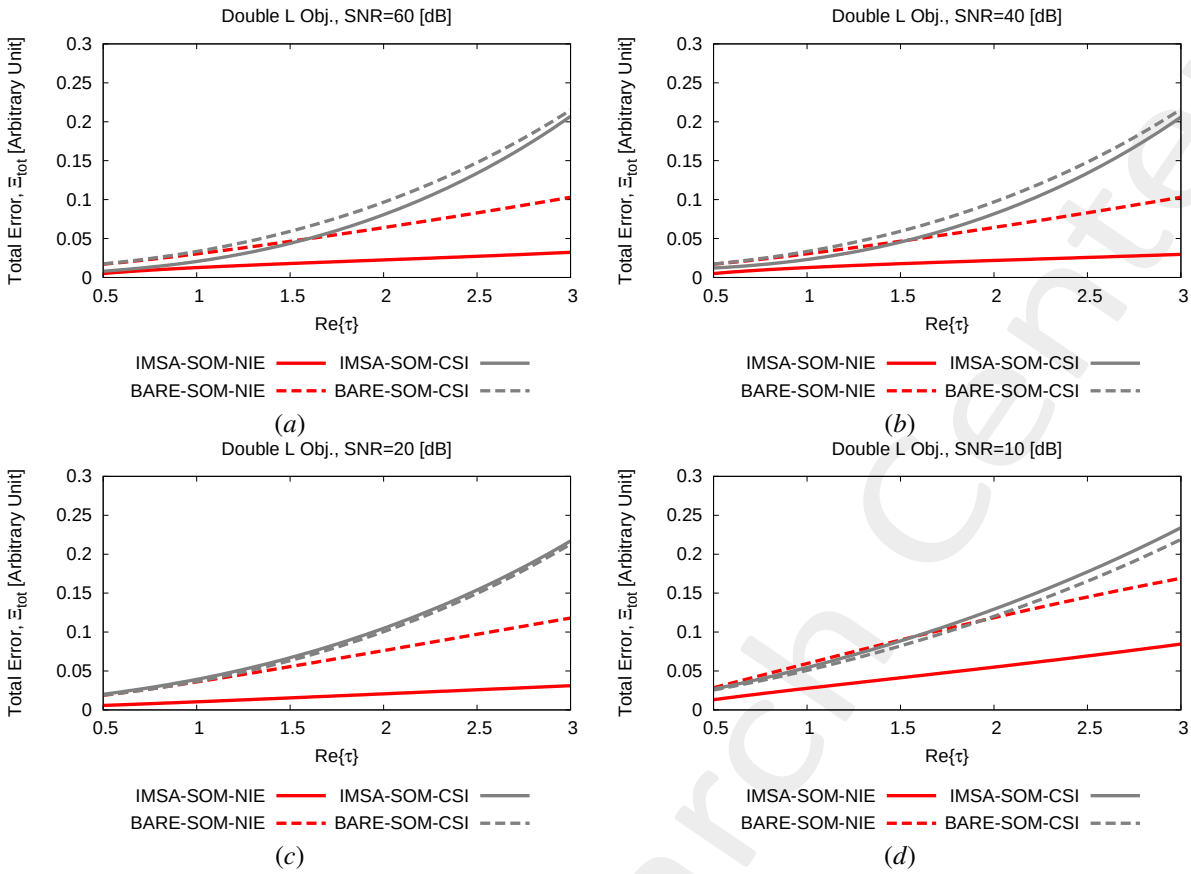

Figure 23: "Double L" Profile - Total error vs. $\Re\{\tau\}$ for $IMSA-SOM-NIE$, $BARE-SOM-NIE$, $IMSA-SOM-CSI$, and $BARE-SOM-CSI$.

2.3 Observations

- In general, the reported results in this section confirm the very good performance of the $IMSA-SOM-NIE$ over state-of-the-art alternatives.

References

[1] G. Oliveri, Y. Zhong, X. Chen, and A. Massa, "Multiresolution subspace-based optimization method for inverse scattering problems," *J. Opt. Soc. Am. A*, vol. 28, no. 10, pp. 2057-2069, Oct. 2011.

[2] X. Ye, L. Poli, G. Oliveri, Y. Zhong, K. Agarwal, A. Massa, and X. Chen, "Multi-resolution subspace-based optimization method for solving three-dimensional inverse scattering problems," *J. Opt. Soc. Am. A*, vol. 32, no. 11, pp. 2218-2226, Nov. 2015.

[3] T. Moriyama, G. Oliveri, M. Salucci, and T. Takenaka, "A multi-scaling forward-backward time-stepping method for microwave imaging," *IEICE Electronics Express*, vol. 11, no. 16, pp. 20140569(1-10), Aug. 2014.

[4] N. Anselmi, G. Oliveri, M. Salucci, and A. Massa, "Wavelet-based compressive imaging of sparse targets," *IEEE Trans. Antennas Propag.*, vol. 63, no. 11, pp. 4889-4900, Nov. 2015.

[5] M. Salucci, G. Oliveri, and A. Massa, "GPR prospecting through an inverse scattering frequency-hopping multi-focusing approach," *IEEE Trans. Geosci. Remote Sens.*, vol. 53, no. 12, pp. 6573-6592, Dec. 2015.

[6] T. Moriyama, M. Salucci, T. Tanaka, and T. Takenaka, "Image reconstruction from total electric field data with no information on incident field," *J. Electromagn. Waves Appl.*, 2016.

[7] M. Salucci, L. Poli, and A. Massa, "Advanced multi-frequency GPR data processing for non-linear deterministic imaging," *Signal Proc.,* vol. 132, pp. 306-318, Mar. 2017.

[8] M. Salucci, L. Poli, N. Anselmi, and A. Massa, "Multifrequency particle swarm optimization for enhanced multiresolution GPR microwave imaging," *IEEE Trans. Geosci. Remote Sens.*, vol. 55, no. 3, pp. 1305- 1317, Mar. 2017.

[9] N. Anselmi, G. Oliveri, M. A. Hannan, M. Salucci, and A. Massa, "Color compressive sensing imaging of arbitrary-shaped scatterers," *IEEE Trans. Microw. Theory Techn.*, vol. 65, no. 6, pp. 1986-1999, Jun. 2017.

[10] G. Oliveri, M. Salucci, N. Anselmi, and A. Massa, "Compressive sensing as applied to inverse problems for imaging: theory, applications, current trends, and open challenges," *IEEE Antennas Propag. Mag.*,vol. 59, no. 5, pp. 34-46, Oct. 2017.

[11] M. Salucci, A. Gelmini, L. Poli, G. Oliveri, and A. Massa, "Progressive compressive sensing for exploiting frequency-diversity in GPR imaging," *J. Electromagn. Waves Appl.*, vol. 32, no. 9, pp. 1164- 1193, 2018.

[12] G. Oliveri, M. Salucci, and N. Anselmi, "Tomographic imaging of sparse low-contrast targets in harsh environments through matrix completion," *IEEE Trans. Microw. Theory Techn.*, vol. 66, no. 6, pp. 2714-2730, Jun. 2018.

[13] M. Salucci, L. Poli, and G. Oliveri, "Full-vectorial 3D microwave imaging of sparse scatterers through a multi-task Bayesian compressive sensing approach," *J. Imaging*, vol. 5, no. 1, pp. 1-24, Jan. 2019.

[14] M. Salucci, G. Oliveri, and A. Massa, "Real-time electrical impedance tomography of the human chest by means of a learning-by-examples method,", *IEEE J. Electromagn., RF, Microw. Med. Biol.*, vol. 3, no. 2, pp. 88-96, Jun. 2019.

[15] G. Oliveri, L. Poli, N. Anselmi, M. Salucci, and A. Massa, “Compressive sensing-based Born iterative method for tomographic imaging,” *IEEE Trans. Microw. Theory Techn.*, vol. 67, no. 5, pp. 1753-1765, May 2019.

[16] I. Merunka, A. Massa, D. Vrba, O. Fiser, M. Salucci, and J. Vrba, "Microwave tomography system for methodical testing of human brain stroke detection approaches," *Int. J. Antennas Propag.,* vol. 2019, ID 4074862, pp. 1-9, 2019.

[17] Y. Zhong, M. Salucci, K. Xu, A. Polo, and A. Massa, “A multi-resolution contraction integral equation method for solving highly non-linear inverse scattering problems,” *IEEE Trans. Microw. Theory Techn.*, vol. 68, no. 4, pp. 1234-1247, Apr. 2020.

[18] M. Salucci, A. Polo, K. Xu, and Y. Zhong, "A multi-resolution computational method to solve highly non-linear inverse scattering problems," *Journal of Physics: Conference Series*, vol. 1476, pp. 1-6, 2020.

[19] N. Anselmi, L. Poli, G. Oliveri, and A. Massa, "Iterative multi-resolution bayesian CS for microwave imaging," *IEEE Trans. Antennas Propag.*, vol. 66, no. 7, pp. 3665-3677, Jul. 2018.

[20] G. Oliveri, P.-P. Ding, and L. Poli "3D crack detection in anisotropic layered media through a sparseness-regularized solver," *IEEE Antennas Wireless Propag. Lett.*, vol. 14, pp. 1031-1034, 2015.

[21] L. Poli, G. Oliveri, P.-P. Ding, T. Moriyama, and A. Massa, “Multifrequency Bayesian compressive sensing methods for microwave imaging," *J. Opt. Soc. Am. A*, vol. 31, no. 11, pp. 2415-2428, 2014.

[22] G. Oliveri, N. Anselmi, and A. Massa, "Compressive sensing imaging of non-sparse 2D scatterers by a total-variation approach within the Born approximation," *IEEE Trans. Antennas Propag.*, vol. 62, no. 10, pp. 5157-5170, Oct. 2014.